



Observed response of marine boundary layer cloud to the interannual variations of summertime Oyashio extension SST front

Naoya Takahashi^{1,5} · Tadahiro Hayasaka¹ · Bo Qiu² · Ryohei Yamaguchi^{3,4}

Received: 15 February 2020 / Accepted: 12 January 2021 / Published online: 30 January 2021
© The Author(s), under exclusive licence to Springer-Verlag GmbH, DE part of Springer Nature 2021

Abstract

Active roles of both sea surface temperature (SST) and its frontal characteristics to the atmosphere in the mid-latitudes have been investigated around the western boundary current regions, and most studies have focused on winter season. The present study investigated the influence of the variation of the summertime Oyashio extension SST front (SSTF) in modulating low-level cloud properties (i.e., low-level cloud cover [LCC], cloud optical thickness [COT], and shortwave cloud radiative effect [SWCRE]) on inter-annual timescales, based on available satellite and Argo float datasets during 2003–2016. First, we examined the mechanism of summertime SSTF variability itself. The strength of the SSTF (S_{SSTF}), defined as the maximum horizontal gradient of SST, has clear inter-annual variations. Frontogenesis equation analysis and regression analysis for subsurface temperature indicated that the inter-annual variations of the summertime S_{SSTF} in the western North Pacific are closely related to the variations of not surface heat flux, but western boundary currents, particularly the Oyashio Extensions. The response of low-level cloud to intensified S_{SSTF} is that negative SWCRE with positive COT anomaly in the northern flank of the SSTF can be induced by cold SST anomalies. The spatial scale of the low-level cloud response was larger than the SST frontal scale, and the spatial distribution of the response was mainly constrained by the pathways of Kuroshio and Oyashio Extensions. Multi-linear regression analysis revealed that the local SST anomaly played largest role in modulating the SWCRE and COT anomalies among the cloud controlling factors (e.g., estimated inversion strength, air-temperature advection) accounting for more than 50% of the variation. This study provides an observational evidence of the active role of local SST anomalies in summertime associated with the western boundary currents to the oceanic low-level cloud.

Keywords Marine boundary layer cloud · Sea surface temperature front · Air–sea interaction · Summertime North Pacific · Interannual variability

1 Introduction

Marine boundary layer (MBL) clouds (e.g., fog, stratus, and stratocumulus), referred to as low-level clouds, tend to occur near the sea surface in the lower troposphere, whose top height is generally lower than 3 km in altitude. They interact strongly with sea surface temperature (SST) via two-way physical processes. Due to their high albedo, they reflect large amounts of shortwave (SW) radiation from the sun back to space, and therefore have a strong cooling effect on the surface of the land and ocean (Hartmann and Short 1980). On the other hand, low-level cloud properties are modulated by SST anomalies through marine atmospheric boundary layer processes. For example, low-level cloud cover (LCC) increases with decreasing SST due to the suppression of the entrainment of dry air from the free troposphere in the boundary layer (Bretherton et al. 2013; Qu

✉ Naoya Takahashi
naoyat@hawaii.edu

¹ Center for Atmospheric and Oceanic Studies, Graduate School of Science, Tohoku University, 6-3 Aoba Aramaki-aza, Aoba-ku, Sendai, Miyagi 9808578, Japan

² Department of Oceanography, University of Hawai'i at Manoa, Honolulu, HI, USA

³ Center for Climate Physics, Institute for Basic Science, Busan, South Korea

⁴ Pusan National University, Busan, South Korea

⁵ Present Address: International Pacific Research Center, School of Ocean and Earth Science and Technology, University of Hawai'i at Manoa, Honolulu, HI, USA

et al. 2015; Kawai et al. 2017). Thus, more humidity can be trapped within the boundary layer if this entrainment is weakened, and LCC increases with decreasing SST itself. As a result, a positive feedback loop exists between variations in both LCC and SST in the North Pacific (NP), especially in summertime (e.g. Norris and Leovy 1994). In the boreal summer (June, July, and August [JJA]) climatology, the LCC and cloud optical thickness (COT) are large over the NP poleward from 40° N and over the south-east of the NP near the Californian coast where the SST is low (contours in Fig. 1a, shaded area and contours in Fig. 1b). In particular, LCC and COT in the NP drastically increase poleward of

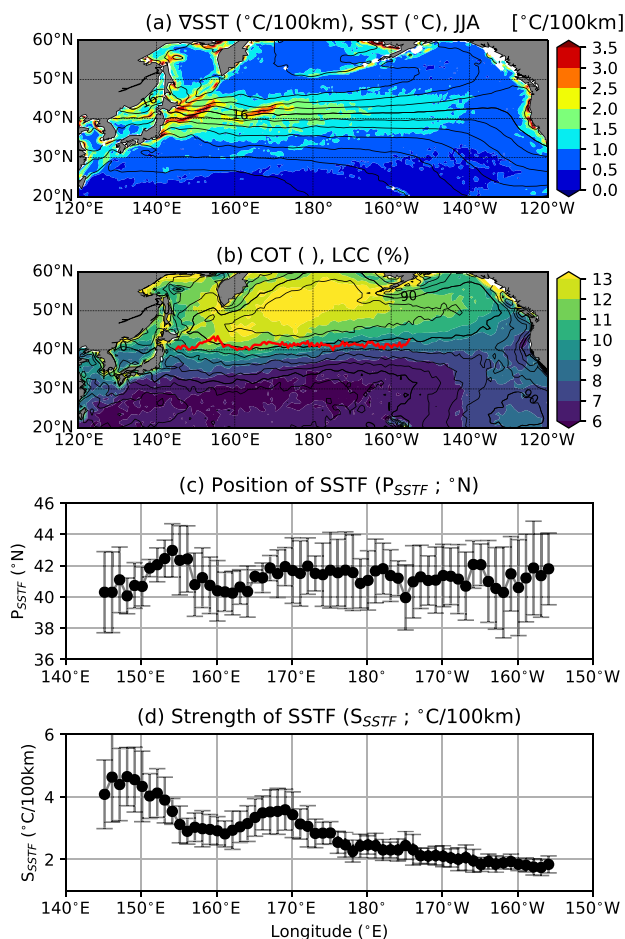


Fig. 1 Climatological conditions in the North Pacific in summertime (June, July, and August [JJA]) from 2003 to 2016. **a** Sea surface temperature (SST; contours, unit: $^{\circ}\text{C}$, contour interval [CI]: 2 K) and its horizontal gradient (∇S_{ST} ; colored areas, unit: $^{\circ}\text{C}/100\text{km}$) from OISST dataset. **b** Cloud optical thickness (COT) of low-level cloud (colored areas, unit: none) and low-level cloud cover (LCC) from a MODIS dataset (contours, unit: %, CI: 5%). Red line indicates the climatological mean position of SST front. Climatological SST front properties in JJA: **c** position (P_{SSTF} , unit: $^{\circ}\text{N}$) and **d** strength of the SST front (S_{SSTF} , unit: $^{\circ}\text{C}/100\text{km}$). Error bars in (c, d) indicate the inter-annual variability

the SST frontal region around 40° N where the horizontal gradient of SST (∇S_{ST}) is larger than 1 $^{\circ}\text{C}/100\text{km}$ (shaded area in Fig. 1a) known as SST front (SSTF). Although a clear correlation has been observed between low-level cloud properties and SST on inter-annual timescales (e.g. Norris and Leovy 1994; Kubar et al. 2012; Koshiro et al. 2017; Myers et al. 2018), their causal relationship is still under debate; this is due to the complex processes in low-level cloud evolution and the difficulty in distinguishing the two-way process within the LCC–SST feedback loop based on casual observational data analysis.

Previous studies have generally found that the mid-latitude ocean plays a passive role in the air–sea interaction process, meaning that SST tends to be forced by the atmospheric variability. In particular, in the summertime mid-latitudes, the mixed-layer depth is so shallow that the SST is strongly forced by surface heat flux variability (e.g. Tanimoto et al. 2003; Cronin et al. 2013). However, recent studies have revealed the active role of the ocean around the western boundary current regions (i.e., the Kuroshio Extension and Gulf Stream) using high-resolution satellite datasets and coupled ocean–atmosphere models (e.g. Nonaka and Xie 2003; Xie 2004; Kwon et al. 2010; Masunaga et al. 2015), meaning that SST can force the atmospheric variability. One of key elements in the SST impacts on the atmosphere is the large ∇S_{ST} formed in the confluence zone of the warm and cold western boundary currents. Two mechanisms have been proposed and widely accepted to explain the influences of SST front on the atmosphere. One is the vertical mixing mechanism (Hayes et al. 1989; Wallace et al. 1989; Chelton 2004). Near sea surface atmosphere destabilizes over the warm flank of the SST front, resulting in promoted vertical momentum mixing and enhanced near surface wind speed. The other is the pressure adjustment mechanism (Lindzen and Nigam 1987; Shimada and Minobe 2011). Surface wind convergence (divergence) occurs over the warm (cold) flank due to high- and low-pressure anomalies generated over the low and high SST anomalies across the front, respectively. These impacts are seasonally dependent (e.g. Minobe et al. 2010) and it is known that heat and moisture supplies are enhanced the most in wintertime because the difference between SST and overlaying atmospheric temperature is maximized (Nakamura and Yamagata 1999; Tanimoto et al. 2003; Tomita et al. 2011).

Some studies have investigated the summertime imprint of the SST front on the atmospheric boundary layer (Tanimoto et al. 2009; Tokinaga et al. 2009; Liu et al. 2014; Kawai et al. 2015, 2019), convective cloud and precipitation (Minobe and Takebayashi 2015; Sasaki and Yamada 2018), and basin-scale atmospheric circulation (Kwon et al. 2010; Frankignoul et al. 2011; Okajima et al. 2014; O’Reilly and Czaja 2015; Yao et al. 2017). For example, Tokinaga et al. (2009) showed seasonal differences in the impact of the

Kuroshio Extension on the vertical development of clouds using both satellite observations and ship-based measurements as a climatological mean, revealing the enhancement of marine fog over the cold flank of the Kuroshio Extension SST front. However, previous studies only focused on the mean state of the summertime low-level cloud properties, paying much less attention to their inter-annual variability. In addition, they also tend to emphasize the importance of warm SST anomalies in wintertime, while cold SST anomalies in summertime can also be important to form the low-level cloud in the North Pacific via modulation of lower atmospheric stability. Kawai et al. (2019) and Jiang et al. (2019) provided the importance of cold SST anomalies to modulate overlaying atmosphere via the pressure adjustment mechanism using ship-based observations and regional atmospheric numerical simulation, suggesting that cold SST anomalies can significantly influence the marine boundary layer clouds in the western North Pacific.

Oceanic dynamics have the potential to drive both the climatological mean state and the inter-annual variation of low-level clouds in summertime through ocean-induced SST anomalies. Recently, Hosoda et al. (2016) investigated the inter-annual variation of the summertime oceanic subsurface temperature in the western, central, and eastern NP based on Argo float observations. They observed a large temperature variability both in the near-surface and in the subsurface up to 600 m depth in the western NP, that is affected by western boundary currents (i.e., the Kuroshio and Oyashio Currents). The findings of Hosoda et al. (2016) also imply the importance of oceanic dynamics for summertime SST despite the strong atmospheric forcing: this motivates us to investigate not only SST but also subsurface oceanic temperature simultaneously in order to reveal the active role of the ocean. We hypothesized that inter-annual variation of SST and the SST front (SSTF) driven by oceanic dynamics has an impact on the local cloud properties despite the strong summertime atmospheric forcing. There are some challenges that must be overcome to reveal the impact of oceanic dynamics on the summertime marine boundary layer and low-level cloud based on observational data analysis. Oceanic forcing to SST is hard to retrieve because the summertime SST is highly sensitive to surface heat flux due to the shallow mixed-layer depth. In this study, to consider oceanic dynamics associated with the western boundary currents, the vertical structure of subsurface temperature determined by Argo float observations was used to diagnose the variability in the Kuroshio or Oyashio Extension. Additionally, we focused on the “frontal” characteristics of SST because the SSTF is a prominent structure that is mainly formed by the western boundary currents (i.e. the oceanic dynamics). For example, the SSTF in the western NP is formed in the confluence region of the Kuroshio and Oyashio Extensions (Nakamura and Kazmin 2003; Kazmin 2016). The objective of the present study was

to reveal the impact of the inter-annual variation of oceanic dynamics on low-level cloud properties—that is, the response of low-level cloud properties to the SSTF variations—based on an observational dataset.

This paper is organized as follows. In Sect. 2, the observational datasets and methods that were used to investigate the properties of the SSTF are described. The properties of the SSTF are also defined. In Sect. 3, we describe the inter-annual variation of the strength of the SSTF and related variability in ocean subsurface temperature (T_{sub}) in the western NP, suggesting that variation in the SSTF is driven by oceanic dynamics. Section 4 describes our investigation into the response of low-level cloud properties to the inter-annual variation of the SSTF. We quantify the contribution of SST to the modulation of low-level cloud properties compared with other controlling factors for low-level cloud using a multi-linear regression model. Section 5 summarizes and discusses our findings.

2 Data and methods

a. Data

In this study, we used daily mean datasets of low-level cloud properties, SST, surface heat flux, and meteorological parameters to investigate the impact of the ocean-driven SSTF around the Oyashio extension on low-level clouds on inter-annual timescales. In addition to these datasets, we also used the monthly-mean datasets of cloud radiative effect (CRE) and oceanic subsurface properties. The period from 2003 to 2016 was analyzed because of the availability of the datasets. This study basically focuses on the boreal summer from June to August, and the monthly-mean states are estimated from the daily data except for CRE and the subsurface properties. Details of each observational dataset are described below.

1. Cloud properties and surface heat flux

To estimate the LCC and the COT of low-level cloud, we used the L3 gridded cloud product (MYD08 D3) from the latest Moderate Resolution Imaging Spectroradiometer (MODIS) release (version 6) from the MODIS instruments on board the Aqua satellite platforms (Platnick 2015) with a horizontal resolution of 1° . Note that this horizontal resolution is not adequate to fully resolve the SST frontal scale impact, such as vertical mixing and pressure adjustment listed before (e.g. Smirnov et al. 2015; Ma et al. 2017). However, the SST impact along the front can be identified as shown in the summertime-mean map of SST and low-level cloud properties (Fig. 1a, b). In addition, the MODIS product is a common one with long-term record

with moderate spatial resolution used in the previous studies (e.g. Masunaga et al. 2016; Miyamoto et al. 2018). Further discussion about spatial–temporal scale dependence of the low-level cloud response to local SST anomaly will be discussed in Sect. 4. Due to the difficulty in estimating the true LCC from passive sensors, the cloud cover was calculated under the random overlapping assumption. Comparison of the cloud cover obtained from the radar and lidar observations with active sensors indicated that the random overlap assumption was reasonable over the mid-latitude oceanic regions compared with other assumptions (Li et al. 2015). Thus, the true LCC was estimated as follows:

$$LCC[\%] = \frac{f_L}{1 - f_M - f_H}, \quad (1)$$

where f_L , f_M , and f_H are the fractions of the scene covered by low-level ($680 \text{ hPa} \leq \text{cloud top pressure [CTP]} < 1000 \text{ hPa}$), mid-level ($440 \text{ hPa} \leq \text{CTP} < 680 \text{ hPa}$), and high-level ($\text{CTP} < 440 \text{ hPa}$) cloud types, respectively. The cloud cover of each of these types was calculated using the histogram of CTP at each grid point within 1 month. Additionally, the “conditional-mean” COT for low-level cloud was calculated using the CTP-COT histograms in each grid with a criterion that CTP is greater than 680 hPa.

Two observational heat flux datasets (SW radiation, long-wave [LW] radiation, sensible heat [SH], and latent heat [LH]) at sea surface were used in this study. To estimate monthly mean radiative fluxes (SW and LW), we used the Clouds and the Earth’s Radiant Energy System (CERES) Energy Balanced and Filled (EBAF) product Edition 4.0 (Loeb et al. 2018; Kato et al. 2018). The variables were calculated using a radiative transfer model initialized using satellite-based cloud and aerosol data and meteorological assimilation data obtained from reanalysis. The variables were also constrained by the observed top-of-atmosphere radiative fluxes. The CERES product was also used to obtain the CRE for SW and LW at the top-of-atmosphere and sea surface, which is defined as the difference between the all-sky radiative flux and clear-sky radiative flux using the radiative transfer model. In the following analysis, we analyzed the SWCRE as one of low-level cloud properties because SWCRE variability depends on the LCC and COT of low-level cloud rather than those of high-level cloud (not shown). The results for LWCRE are also not shown here because its response and variability are smaller than those of SWCRE by one order of magnitude. Global ocean-surface heat flux products were obtained from the daily mean turbulent fluxes dataset of the Objectively Analyzed air-sea Heat Fluxes (OAFlux) project of the Woods Hole Oceanographic Institution (Yu et al. 2008). The OAFlux products are constructed not from a single data source, but from an optimal blending of satellite retrievals and three atmospheric

reanalysis datasets. The horizontal resolutions of the CERES and OAFlux products are 1° in longitude and latitude.

2. Oceanic properties

The objectively analyzed daily mean SST of the National Oceanic and Atmospheric Administration (NOAA) Optimum Interpolation version 2 (OISST; Reynolds et al. 2002) was used as the SST dataset. Monthly mean SST was calculated by averaging from the interpolated daily dataset with a horizontal resolution of 0.25° . To assess the interannual variability of oceanic subsurface structures associated with the strength of the SST front, we used a monthly mean three-dimensional temperature dataset based on Argo profiling float observations (Argo 2000). The Roemmich–Gilson (RG) Argo Climatology dataset provided by the Scripps Institution of Oceanography (Roemmich and Gilson 2009) was used. The horizontal resolution of the RG product is 1° , and the vertical resolution varies with depth (e.g., 25 m resolution from a depth of 10 to 200 m), and analysis was conducted using a two-dimensional optimal interpolation method on pressure surfaces for temperature and salinity. To calculate the mixed layer depth (MLD), we used the Monthly Isopycnal/Mixed-layer Ocean Climatology (MIMOC; Schmidt et al. 2013) dataset estimated mostly by Argo float observation, supplemented by ship observations and conductivity-temperature-depth profile data.

3. Meteorological properties

To estimate the variability of the meteorological field associated with the inter-annual variations of low-level cloud and SSTF, we used ERA5 reanalysis hourly data (Hersbach et al. 2020) with a horizontal resolution of 0.25° and 137° vertical levels whose resolution is finer than that of ERA-Interim (Dee et al. 2011). Monthly mean data of air temperature at 700 and 1000 hPa, horizontal wind at 1000 hPa, and sea-level pressure were used to calculate the EIS and T_{adv} as a proxy for LCC controlling factors. EIS was calculated following the method of Wood and Bretherton (2006), showing the inversion strength at the top of planetary boundary layer given the air temperature at 700 hPa and at the sea surface. T_{adv} was calculated $\mathbb{W}_{adv} [K/day] = -u_{1000hPa} \partial T_{1000hPa} / \partial x - v_{1000hPa} \partial T_{1000hPa} / \partial y$ where $T_{1000hPa}$, $u_{1000hPa}$ and $v_{1000hPa}$ are the temperature, zonal wind speed, and meridional wind speed at 1000 hPa, respectively. Instead of $T_{1000hPa}$ and wind at 1000 hPa, the SST and wind at 10 m could be used, respectively. However, the computed temperature advections were not significantly different and did not depend on the variables used (Zelinka et al. 2018). Additionally, the vertical pressure velocity and relative humidity at 700 hPa (ω_{700} and RH_{700} , respectively) were also used as the controlling factors for the low-level

cloud properties. To obtain the monthly-mean states of EIS and T_{adv} , we first calculated the hourly values at each grid point, and then calculated monthly-mean values. Compared with the calculation method using monthly-mean datasets, the estimated monthly-mean states of EIS and T_{adv} are significantly different due to the large sub-monthly variations in air-sea temperature and near sea surface winds around the oceanic frontal zone (e.g. Miyamoto et al. 2018; Sasaki and Yamada 2018; Ogawa and Spengler 2019; Masunaga et al. 2020).

b. Methods

The position of the SSTF (P_{SSTF}) was defined as the latitude where the horizontal gradient of the SST has a maximum value for each month and each longitude bin of 0.25° width. To extract the properties of the SSTF associated with the Oyashio extension (Isoguchi et al. 2006), we searched for the P_{SSTF} in the latitude range of $35\text{--}45^\circ\text{N}$. The strength of the SST front (S_{SSTF}) was defined as the maximum horizontal gradient of the SST. Mathematically, S_{SSTF} can be expressed as:

$$S_{SSTF}(x, t) [^\circ\text{C}/100\text{ km}] = [\max(\nabla\text{SST}(x, y, t))]_{x,t} \quad (2)$$

where x , y , and t are the longitude, latitude, and time, respectively; and $[\]_{x,t}$ denotes searching for the maximum value of the horizontal gradient of the SST for the longitude bin (x) and time (t). As an example, we plotted the climatological P_{SSTF} and S_{SSTF} in JJA (Fig. 1c and d).

To confirm that the SSTF properties, in particular S_{SSTF} , are determined by oceanic forcing rather than atmospheric forcing (i.e., the impact of SST/SSTF on the atmosphere), we investigated the frontogenesis/frontolysis process (i.e., strengthen/weaken in S_{SSTF}) in the western NP using the following frontogenesis equation (Tozuka and Cronin 2014; Ohishi et al. 2017; Tozuka et al. 2017):

$$\frac{\partial}{\partial t} \left(\frac{\partial\text{SST}}{\partial y} \right) = \frac{\partial}{\partial y} \left(\frac{Q}{\rho_0 C_p H_{mix}} \right) + \frac{\partial}{\partial y} (\text{oceanic}), \quad (3)$$

where Q is the net sea-surface heat flux, ρ_0 is the typical sea water density, C_p is the specific heat at a constant pressure, H_{mix} is the MLD derived from the MIMOC dataset, *oceanic* is the SST tendency term derived from the oceanic dynamics (i.e., other than the surface heat flux term; horizontal advection, vertical mixing, etc.). The $\frac{\partial}{\partial y}(\text{oceanic})$ term in Eq. 3 is calculated as the residual of the equation. This equation was based on a simplified mixed-layer temperature budget (Moisan and Niiler 1998) and assumes that SST is equivalent to the temperature of the mixed layer. In the SSTF region in the western NP, the horizontal gradient of SST is dominated by the meridional component rather than the zonal component. Thus, we only considered the meridional

component of the SST gradient in Eq. 3, and investigated the variation of S_{SSTF} and the underlying physical process that modulate it using the above frontogenesis equation.

3 Mechanism of SSTF variations in the summertime western NP

a. Climatology of SSTF Properties in Summertime from 2003 to 2016

Figure 1c, d show the climatological zonal distributions of P_{SSTF} and S_{SSTF} in the boreal summer (JJA) NP and their standard deviations (SD) of the inter-annual variability. The figure shows some zonal differences in SSTF properties between the parts to the west and east of 170°E , which are respectively called the western NP (WNP) and central NP (CNP) hereafter. The zonal differences in the climatological P_{SSTF} are found to be not as large as those for S_{SSTF} ; however, the SD of the P_{SSTF} was much smaller in the WNP than in the CNP (Fig. 1c), implying the stable and unstable SSTF in the WNP and CNP, respectively. Second, the climatological S_{SSTF} is stronger in the WNP than in the CNP (i.e., $3\text{--}5^\circ\text{C}/100\text{ km}$ in the WNP, $<3^\circ\text{C}/100\text{ km}$ in the CNP; Fig. 1d). Additionally, there are two peaks for S_{SSTF} at around 150 and 170°E , respectively. These correspond to the Oyashio extension SSTFs trapped by bottom topography, called the Isoguchi Jet (IJ) 1 and IJ2 regions (Isoguchi et al. 2006). Qiu et al. (2017) suggested that these SSTFs vary independently on decadal timescales, and other studies showed their close relationship with the variability of the Kuroshio Extension (e.g. Sugimoto et al. 2014), which is one of the strongest warm western boundary currents in the world and has a deep vertical structure with a thickness of about 600 m (Qiu 2001). Additionally, observational studies have examined the relative contributions of atmospheric forcing (i.e., surface heat flux) and oceanic forcing (i.e., subsurface temperature advection, vertical mixing across the base of mixed layer, etc.) to the SST tendency in summertime; for example, oceanic forcing has been shown to be dominant in the WNP (Wu and Kinter 2010; Hosoda et al. 2016). Figure 2 displays a longitude–depth cross-section of the SD of T_{sub} in JJA along the SST frontal region ($35\text{--}45^\circ\text{N}$) estimated from the RG product. Here, the large temperature variability in the WNP reaches to a deeper depth of 400 m than that in the CNP of 100 m , suggesting that the oceanic forcing and the surface heat flux forcing are dominant cause of the temperature variability in the WNP and CNP, respectively (Hosoda et al. 2016). In this study, we set our target region in WNP as the IJ2 region from 160° to 170°E because the summertime SSTF in this region is likely driven by oceanic dynamics rather than atmospheric forcing.

b. Inter-annual variation of subsurface temperature and SSTF properties

The time series of the SSTF properties for all months and only JJA-mean state in the IJ2 region are shown in Fig. 3. The inter-annual variation of the SSTF properties in the IJ2 region was relatively small (SD of P_{SSTF} : 0.83°N for all months and 0.62°N for JJA only), and cannot be resolved by the coarse grid of the low-level cloud dataset (i.e. horizontal resolution of 1°). The seasonal variation of P_{SSTF} was unclear. In contrast, S_{SSTF} in the IJ2 region had a clear seasonality; S_{SSTF} had minimum and maximum values in summertime and wintertime, respectively (not shown), consistent with the results of previous studies (Kazmin 2016; Tozuka et al. 2017, 2018). Interestingly, clear inter-annual variation of S_{SSTF} was also observed in the summertime-mean state, e.g., a negative anomaly from 2005 to 2008 and a positive anomaly from 2009 to 2011 (Fig. 2b). This kind of low-frequency variation of the Oyashio extension SSTF is possibly modulated by oceanic process (Frankignoul et al. 2011; Sugimoto et al. 2014; Qiu et al. 2017). Correlation coefficient with the indices of P_{SSTF} and S_{SSTF} are almost zero ($r=0.02$), thus the variations of these indices are considered to be independent. Hereinafter, we focus on only the inter-annual variation of S_{SSTF} and the response of low-level cloud to this parameter, rather than the P_{SSTF} . Note that the P_{SSTF} anomaly in summertime of 2007 has large negative values (i.e. located further south from the climatological mean position) due to an influence of oceanic eddies (not shown). Oceanic eddies around the front possibly induce large biases in the low-level cloud response to the front, however, results shown later do not change whether the period of 2007 is included or not.

Figure 4 displays the regressions of SST and T_{sub} onto the summertime S_{SSTF} in the IJ2 region ($160\text{--}170^\circ\text{E}$; Fig. 4a, c) and a part of the CNP ($155\text{--}165^\circ\text{W}$; Fig. 4b, d), indicating the oceanic state at the sea surface and in the subsurface when S_{SSTF} is increased by one standard deviation ($1\sigma=0.23^\circ\text{C}/100\text{ km}$). In Fig. 4, the x-axis is modified to relative latitude from the JJA-mean P_{SSTF} in each part of the SSTF region. As expected, the response of SST to the strengthen of S_{SSTF} (ΔSST) was negative (colder) in the northern flank of the SSTF (Fig. 4a). ΔSST in the southern flank is positive but not significant. Although the spatial patterns of ΔSST were similar in the IJ2 region and the CNP (Fig. 4b), the spatial patterns of the response to T_{sub} (ΔT_{sub}) were notably different in these two regions. In the IJ2 region, the meridional contrast of ΔT_{sub} across the position of SSTF was found both at the near sea surface and in the deeper part (Fig. 4c). Additionally, a warm ΔT_{sub} appeared from a depth of 100–600 m in the southern flank around -10° (Fig. 4c), corresponding to the relative position of Kuroshio Extension. In contrast, the significant

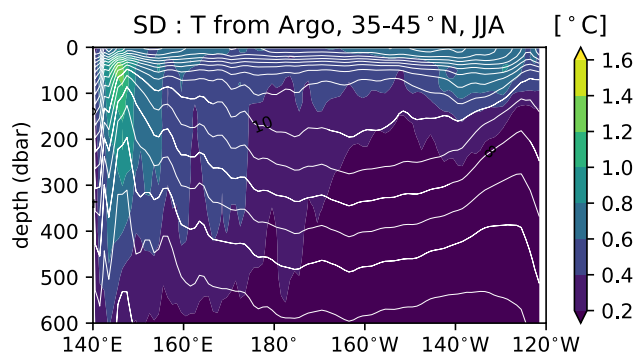


Fig. 2 The standard deviation (SD) of the inter-annual variation of subsurface temperature obtained from Argo observation at latitudes of $35\text{--}45^\circ\text{N}$ for June, July, and August (JJA) in 2003–2016 (colored areas, unit: $^\circ\text{C}$). The climatological mean of subsurface temperature is also plotted (contours, unit: $^\circ\text{C}$, CI: 1°C)

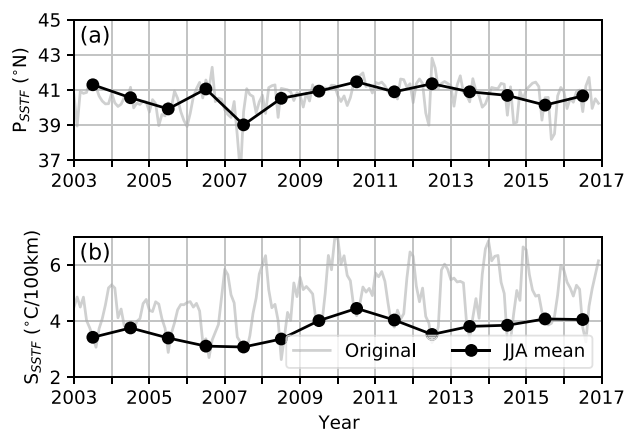


Fig. 3 Time series of mean **a** position of the sea surface temperature front (P_{SSTF}) and **b** strength of the sea surface temperature front (S_{SSTF}) in the Isoguchi Jet 2 region ($160\text{--}170^\circ\text{E}$). Thin and thick lines indicate the original time series and June, July, and August (JJA)-mean values, respectively. Horizontal dashed lines show the climatological mean values of JJA-mean sea surface temperature front properties

meridional contrast of ΔT_{sub} in the CNP does not appear in the subsurface, implying that changes in SST tend to be strongly controlled by the surface heat flux forcing (Hosoda et al. 2016). In other words, the meridional contrast of ΔT_{sub} in the deeper part of the IJ2 region presents the observational evidence for the ocean-induced SST and SSTF properties even in the summertime. Figure 5 shows the spatial distribution of summertime ΔSST regressed onto S_{SSTF} of the IJ2 region. As shown in Fig. 4a, a warm (cold) ΔSST appears in the southern (northern) flank of the SSTF when S_{SSTF} is increased (Fig. 5). Additionally, the ΔSST s spread widely away from the IJ2 region. For example, cold ΔSST s appear in the northern flank of the IJ2 SSTF with a zonal expansion along the path of the Oyashio Extension. On the other side, warm ΔSST s appear from 140° to 170°E , which is along

the path of the Kuroshio Extension. These spatial characteristics imply that the ΔS_{SSTF} and the strengthening process of S_{SSTF} in the summertime IJ2 region are closely related to the Kuroshio and Oyashio Extensions.

- iii. Mechanisms of frontogenesis in the IJ2 region; atmospheric forcing vs oceanic forcing

We investigated how the summertime SSTF properties were determined, based on the frontogenesis equation (Eq. 3). Figure 6 shows the seasonal evolution of each term in the frontogenesis equation from May to September. Note that, in Fig. 6, a positive (negative) rate indicates frontogenesis (frontolysis) and the meridional gradient of SST ($\partial S_{SST}/\partial y$) is always negative in the IJ2 region. As described above, S_{SSTF} in the IJ2 region is the smallest in summertime and strongest in wintertime (e.g., Tozuka et al. 2018). Frontolysis occurs in JJA due to the surface net heat flux (HF) term (red line), which weakens the S_{SSTF} (Fig. 6). In contrast, the oceanic term (OCN; blue line) always induces frontogenesis in the IJ2 region. The results shown in Fig. 6

imply that the HF term is a dominant factor modulating summertime frontolysis in the climatological seasonal cycle.

Figure 7a displays the mean meridional distribution of $\partial S_{SST}/\partial y$ and that of the mean meridional gradient of heat flux ($\partial Q/\partial y$) in the IJ2 region. The minimum $\partial S_{SST}/\partial y$ and maximum $\partial Q/\partial y$ occur close to the position of the SSTF. Note that a positive $\partial Q/\partial y$ means more heat release or less heat input in the south of SSTF as compared to that in the north; frontolysis process. To further investigate the relationship between the HF term and S_{SSTF} on inter-annual timescales, Fig. 7b displays a scatter plot of $\partial S_{SST}/\partial y$ vs $\partial Q/\partial y$ on the SSTF in JJA from 2003 to 2016, indicating the relationship between the strength of the SSTF ($\sim \partial S_{SST}/\partial y$) and the frontolysis by surface heat flux forcing ($\sim \partial Q/\partial y$) on inter-annual timescales. Note that the meridional gradient of MLD has a negligible effect on the frontolysis in summertime (not shown). A significant negative correlation (~ -0.85) can be seen between $\partial S_{SST}/\partial y$ and $\partial Q/\partial y$, suggesting that more frontolysis (i.e., positive values of $\partial Q/\partial y$) occurs when the SSTF is strengthened (i.e., negative values of $\partial S_{SST}/\partial y$). This indicates that a frontolysis does not decrease S_{SSTF} , but that

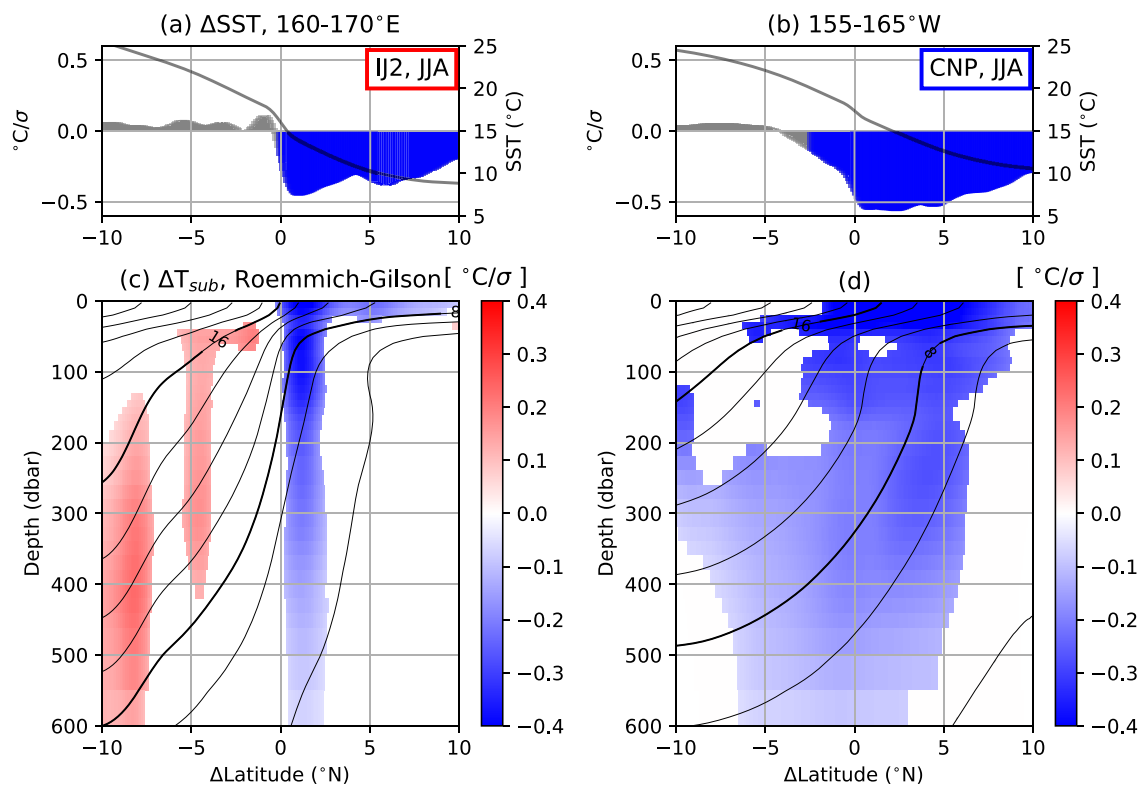


Fig. 4 a Meridional distribution of the response of the sea surface temperature (SST) to the increase of the strength of the sea surface temperature front by one standard deviation (bar corresponding with the left y-axis) and the climatological mean value of the SST (line corresponding with the right y-axis) in the Isoguchi Jet 2 region. The x-axis is the shifted latitude based on the position of the sea surface temperature front (P_{SSTF}). c Latitude–depth cross-section of

the response of the subsurface temperature (T_{sub}) in the Isoguchi Jet 2 region obtained from the Roemmich–Gilson product of Argo float observation from 2004 to 2016. Responses within the 95% confidence interval are displayed in color. Contour lines are climatological values of subsurface temperature (CI: 2 °C). b, d are the same as (a, c), respectively, but for the central North Pacific (CNP; 155–165° W)

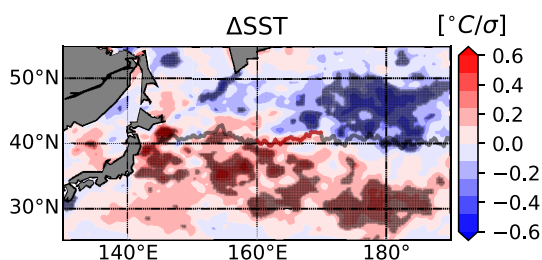


Fig. 5 The responses of the sea surface temperature (SST) ($^{\circ}\text{C}$) at each grid point to the increased strength of the sea surface temperature front in the Isoguchi Jet 2 region (at $160\text{--}170^{\circ}\text{E}$) by one standard deviation. The black line (red points) shows the climatological mean position of the sea surface temperature front (in the Isoguchi Jet 2 region). Grid boxes with a black cross indicate responses within the 95% confidence interval

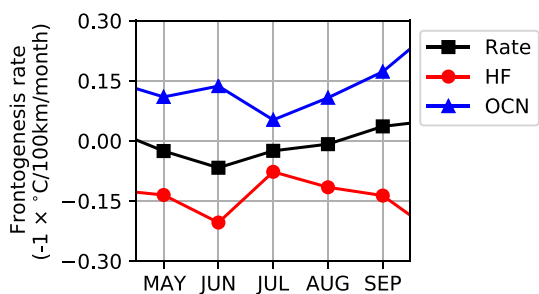


Fig. 6 The seasonal variation from May to September of each term of the frontogenesis equation in the Isoguchi Jet 2 region, calculated according to Tozuka and Cronin (2014). The surface heat flux term calculated based on the meridional gradient of net heat flux (HF; red line), the oceanic term (OCN; solid line), and the total frontogenesis rate (Rate; black line) are plotted. A positive (negative) value indicates frontogenesis (frontolysis), meaning that the strength of the sea surface temperature front is increased (decreased) by the frontogenesis (frontolysis) process in each month

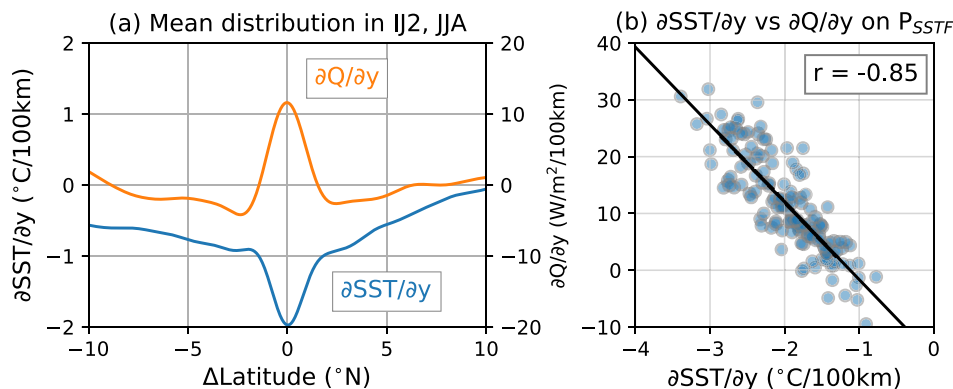


Fig. 7 **a** Mean meridional distribution of the meridional gradient of the sea surface temperature ($\partial\text{SST}/\partial y$; unit: $^{\circ}\text{C}/100\text{km}$; left y -axis) and that of net heat flux ($\partial Q/\partial y$; unit: $\text{W}/\text{m}^2/100\text{km}$; right y -axis) close to the position of the sea surface temperature front (P_{SSTF}) in the Isoguchi Jet 2 (IJ2) region in June, July, and August (JJA). Down-

ward heat flux is defined as positive; thus, a positive $\partial Q/\partial y$ indicates that a small heat input (or large heat release) occurs in the south of the IJ2 region, suggesting frontolysis. **b** Scatter plots of $\partial\text{SST}/\partial y$ vs $\partial Q/\partial y$ from 2003 to 2016 in JJA. The correlation coefficient between $\partial\text{SST}/\partial y$ and $\partial Q/\partial y$ is displayed in the upper right

an increased S_{SSTF} induces more frontolysis by modulating the heat release from the sea surface, reflecting the active role of the ocean in the modulation of surface heat flux. The zonal distribution of the correlation coefficients in Fig. 8 is similar to that shown in Fig. 7b, and the correlation coefficients with each component of heat flux are also displayed. The correlation between $\partial Q/\partial y$ and $\partial\text{SST}/\partial y$ was significantly negative in both the IJ2 region and in the western part from 170°W , where the climatological mean S_{SSTF} is greater than $1.5^{\circ}\text{C}/100\text{km}$ (Fig. 1a). Furthermore, the correlation coefficient between SH and LH is also significantly negative, indicating that S_{SSTF} is effectively damped by the turbulent flux due to the SST anomaly itself. Unlike the western part including the IJ2 region, there was no significant correlation between $\partial Q/\partial y$ and $\partial\text{SST}/\partial y$ in the CNP; the eastern part from 170°W . The relationship between HF and SST (or $\partial Q/\partial y$ and $\partial\text{SST}/\partial y$) that acts to damp the SST (SSTF) has been recognized as an active role in SST (Tanimoto et al. 2003), which has been confirmed in the western part from the date line. Thus, we can assume that, in the IJ2 region, the inter-annual variation of S_{SSTF} is mainly driven by the oceanic forcing, rather than the heat flux forcing. Hereinafter, we regarded the regressions of low-level cloud properties onto S_{SSTF} as the impact of ocean-driven SST anomalies on the low-level cloud.

4 Response of summertime low-level cloud properties to S_{SSTF} in the IJ2 region

SST frontal characteristics (i.e., S_{SSTF} and P_{SSTF}) have been recognized as the ocean-induced factors modulating atmospheric conditions in the mid-latitudes, particularly for wintertime, including the storm tracks (Nakamura et al. 2004;

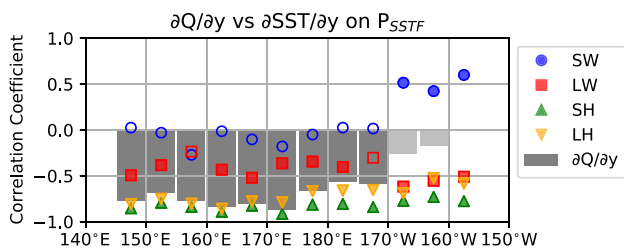


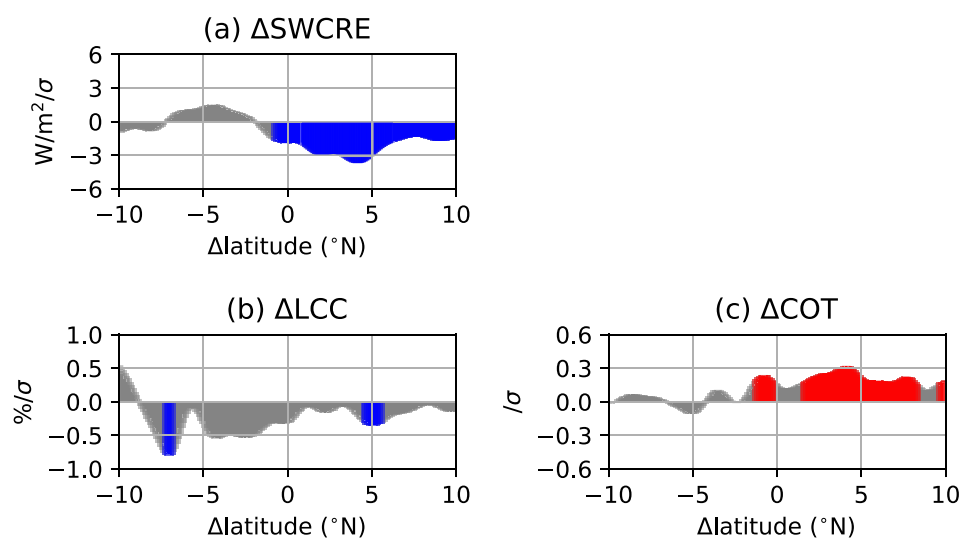
Fig. 8 Correlation coefficients between $\partial S_{SSTF}/\partial y$ and the meridional gradients of each flux term (shortwave [SW] radiation: blue, long-wave [LW] radiation: red, sensible heat [SH]: green, and latent heat [LH]: orange) and the correlation coefficients between $\partial S_{SSTF}/\partial y$ and the meridional gradient of net heat flux ($\partial Q/\partial y$) (gray bars) close to the position of the sea surface temperature front (P_{SSTF}) in the Itoiguchi Jet 2 region in June, July, and August (JJA). Correlation coefficients were calculated for every 5° longitudinal bin from 145° E eastward. For all colored markers and gray bars, the correlation coefficients are within the 95% confidence interval

Ogawa et al. 2012, 2016; Masunaga et al. 2016; Parfitt and Seo 2018) and vertical cloud distributions (Tanimoto et al. 2009; Tokinaga et al. 2009; Liu et al. 2014; Kawai et al. 2015, 2019). In the previous section, we confirmed that the inter-annual variation of the summertime S_{SSTF} in the IJ2 region is likely driven by oceanic forcing from the Kuroshio and Oyashio Extensions. In this section, we estimate the response of low-level cloud properties to the increased S_{SSTF} in the IJ2 region. To do this, we calculated the linear regression coefficient of each cloud variable and the controlling factor at every grid point to the inter-annual variation of the mean S_{SSTF} in the IJ2 region. We recorded the meridional distributions of the responses of low-level cloud properties (i.e., LCC, COT of low-level cloud, and SWCRE at the sea surface) to the S_{SSTF} index in JJA (Fig. 9). We found a distinct pattern in these responses, particularly for

SWCRE, in the northern flank of the SSTF. In the northern flank, $\Delta SWCRE$ was negative over the cold ΔS_{SST} (Fig. 9a), mainly due to the positive ΔCOT (Fig. 9c), rather than the ΔLCC . The opposite was apparent for the negative ΔLCC in the northern flank; however, the ΔLCC in this region showed lower statistical significance. While the responses were not significant in the southern flank, $\Delta SWCRE$ was positive over the warm ΔS_{SST} (Fig. 9a) mainly due to the negative ΔLCC (Fig. 9b). Similar results are displayed in Fig. 10, except for their horizontal distributions. A common feature of all three low-level cloud properties is that the responses to S_{SSTF} appear in a wide region not confined to around the IJ2 region. This spatial feature is similar to the results for SST (Fig. 5) associated with the western boundary currents, that is, the paths of Kuroshio and Oyashio Extensions. The positive response of ΔLCC to ΔS_{SST} in the southern flank of the SSTF is similar to the observations of previous studies described in Sect. 1 (Norris and Leovy 1994; Norris et al. 1998; Bretherton et al. 2013). Similar to the response of LCC to SST, COT can also be modulated by changes in the entrainment process of dry air from the free troposphere into the boundary layer associated with an SST anomaly; COT increases with decreasing SST (Terai et al. 2016, 2019), which is consistent with the positive ΔCOT in the northern flank of the SSTF observed in the present study (Figs. 9c and 10c).

Low-level cloud properties are modulated by not only the local SST but also other atmospheric variables, as reported in many previous studies (Qu et al. 2015; Seethala et al. 2015; Myers and Norris 2016; McCoy et al. 2017; Klein et al. 2017; Miyamoto et al. 2018; Zelinka et al. 2018). For example, they investigated the contribution from the various controlling factors listed above to assess the response of low-level cloud to global warming (Qu et al. 2015; Zhai

Fig. 9 As in Fig. 4a, but for **a** the shortwave cloud radiative effect (SWCRE) (unit: W/m^2), **b** cloud optical thickness (COT; unit: none), and **c** low-level cloud cover (LCC; unit: %). The standard deviation of the strength of the sea surface temperature front is shown in the upper right



et al. 2015; Myers and Norris 2016; Brient and Schneider 2016; Terai et al. 2016; McCoy et al. 2017). The consensus is that the formation of a large amount of low-level cloud is favored by strong temperature inversions at the top of cloud (Wood and Bretherton 2006), cool SST (Bretherton et al. 2013), weak subsidence (Myers and Norris 2013), and enhanced turbulence with upward heat flux induced by cold-air advection near the sea surface (Norris and Iacobellis 2005). Thus, we attempted to quantify the contributions of the different controlling factors separately using the multi-linear regression analysis method that was employed in the studies referenced above. Figure 11 shows the responses of four other LCC controlling factors—namely EIS, T_{adv} , RH_{700} , and ω_{700} —to S_{SSTF} ; all of these four factors have been widely used. When S_{SSTF} is increased, ΔEIS is negative in the southern flank of the SSTF, and the opposite in the northern flank (Fig. 11a). Negative ΔEIS caused by a positive ΔSST indicates unstable conditions in the lower troposphere, which is unfavorable for the formation of low-level cloud (Klein and Hartmann 1993; Wood and Bretherton 2006; Kawai et al. 2017). Although the low-level cloud tends to form with cold T_{adv} through a destabilization process in the atmospheric boundary layer (Wood 2012), ΔT_{adv} was observed to be negative around the SSTF (Fig. 11b). For other atmospheric factors that control LCC, ΔRH_{700} was negative (positive) in the southern (northern) flank (Fig. 11c) and $\Delta \omega_{700}$ was positive in the southern flank (Fig. 11d) indicating strong subsidence or weak updraft. Strong subsidence and a dry free-troposphere are also unfavorable conditions for low-level cloud formation (Bretherton et al. 2013; Myers

and Norris 2013, 2015). In conclusion, almost all of the LCC controlling factors responded simultaneously to the inter-annual variation of S_{SSTF} and acted to change the low-level cloud properties toward the same sign around the IJ2 SSTF region, except for T_{adv} .

To quantify the relative contributions of the controlling factors to the properties of low-level cloud (Figs. 9 and 10), a multi-linear regression (MLR) analysis was conducted. All variables were spatially interpolated to the coarsest common grid of 1° for the low-level cloud products. The response of low-level cloud properties (referred to as C ; i.e. LCC, COT, or SWCRE) to the increased S_{SSTF} is expressed as follows:

$$\Delta C = \frac{\partial C}{\partial S_{SSTF}} = \sum_i \frac{\partial C}{\partial x_i} \frac{\partial x_i}{\partial S_{SSTF}},$$

where x_i is a controlling factor, namely, SST, EIS, T_{adv} , RH_{700} , or ω_{700} . The partial derivatives of the low-level cloud properties were calculated using a multi-linear regression approach similar to that used in previous studies (summarized in Klein et al. 2017). To construct the MLR model to estimate the response of low-level cloud to the five LCC controlling factors, we used the anomalies of all cloud parameters and predictors from each seasonal mean value in JJA at each grid point in the western NP region ($130\text{--}170^\circ$ E, $30\text{--}55^\circ$ N). Due to multicollinearity between the SST and EIS, this model possibly underestimates the contributions from the SST and EIS. Then, from original EIS variability, we subtracted EIS regressed onto SST before calculating the slopes in the MLR model. Table 1 shows the regression

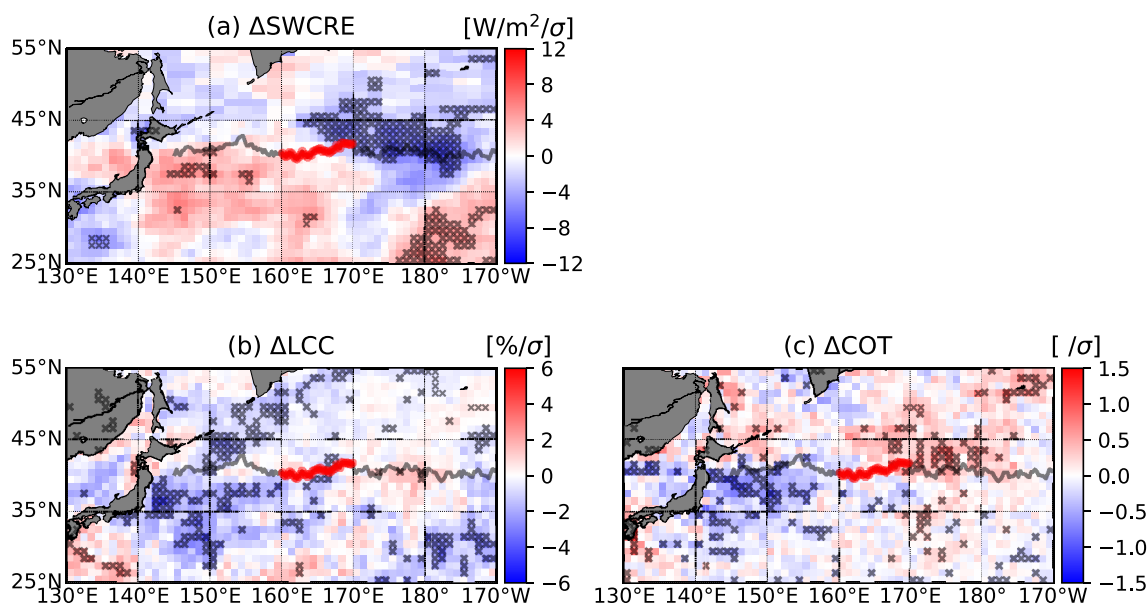
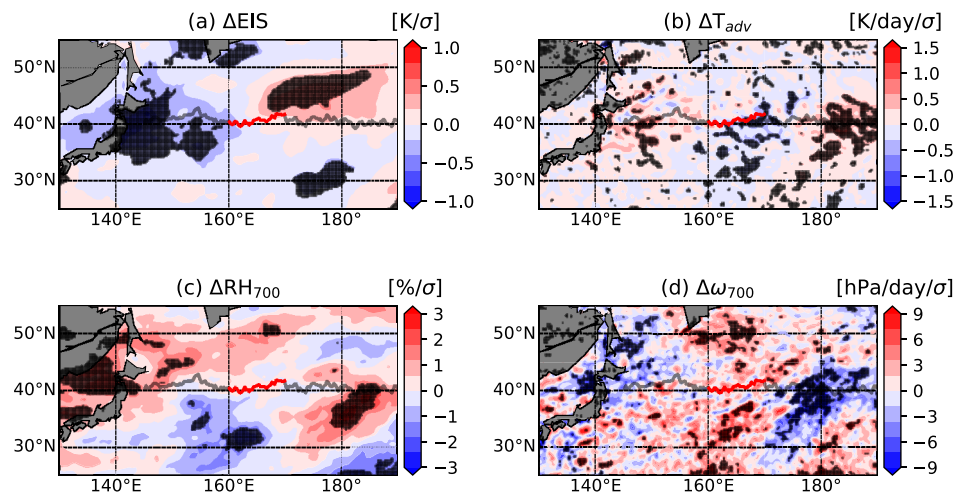


Fig. 10 As in Fig. 5, but for **a** the shortwave cloud radiative effect (SWCRE; unit: W/m^2), **b** low-level cloud cover (LCC; unit: %), and **c** cloud optical thickness (COT; unit: none)

Fig. 11 As in Fig. 5, but for **a** estimated inversion strength (EIS) (unit: K), **b** horizontal air-temperature advection (T_{adv}) (unit: K/day), **c** relative humidity at 700 hPa (RH_{700} ; unit: %), and **d** vertical pressure velocity at 700 hPa (ω_{700} ; unit: hPa/day)



slopes calculated using the constructed MLR model for LCC, COT, and SWCRE. Except for the removal of multicollinearity between the SST and the EIS, this process is similar to the procedures used in the previous studies (e.g., Klein et al. 2017). The signs of the slopes are also consistent with the physical mechanisms confirmed in the previous observational and numerical simulation studies using CMIP5 model outputs (e.g. Klein et al. 2017). For example, the negative slopes of LCC and COT to SST suggest that, when SST is low, low-level cloud appears more frequently and becomes more dense due to the suppression of the entrainment process of dry air from the free troposphere into the moist boundary layer (Bretherton et al. 2013; Qu et al. 2015). The variances of the three MLR models to the actual response of each low-level cloud variable are 66% for LCC, 40% for COT, and 68% for SWCRE. We also calculated the confidence interval from 5 to 95% of each slope, but the interval for each slope was smaller than the slope value itself by one order of magnitude. The coefficients for LCC and COT are calculated from the daily-mean states, but the results are not significantly different from those using the monthly-mean states (not shown). These are also consistent with Miyamoto et al. (2018), which focused on a different western boundary current region, the Agulhas Return Current. We recorded comparisons between the responses of low-level cloud to S_{SSTF} calculated directly by linear regression (shown in Fig. 9) and those estimated using the MLR model (“Total”) around the IJ2 SSTF (Fig. 12). The figure also shows the contributions of each controlling factor calculated based on the slopes of each low-level cloud variable output by the MLR model (Table 1). These contributions show that SST is a primary controlling factor for all cloud responses. In particular, the ratio of the actual responses to the SST contribution was 50% for ΔCOT and 103% for $\Delta SWCRE$ in the northern flank of the IJ2 SSTF (i.e. Meridional mean from Δ latitude of 0° to $+5^\circ$). In contrast, the

responses of low-level cloud properties in the southern flank, where the cloud responses are not significant (Figs. 9 and 10), could not be estimated well. Takahashi and Hayasaka (2020) suggested that T_{adv} is likely to be a main driver of the LCC variability in the WNP on the intra-seasonal time-

Table 1 Calculated regression slopes for each cloud variable for each predictor in the multi-linear regression model of LCC, COT, and SWCRE

	$\partial C/\partial SST$	$\partial C/\partial EIS$	$\partial C/\partial T_{adv}$	$\partial C/\partial RH_{700}$	$\partial C/\partial \omega_{700}$
LCC	-3.18	5.72	-2.22	0.23	0.05
COT	-0.29	0.16	-0.13	0.01	0.01
SWCRE	7.89	-6.92	1.94	-0.63	0.04

LCC: low-level cloud cover, COT: cloud optical thickness, SWCRE: shortwave cloud radiative effect

scales (about 20–100 days), however, in the present study, we observed SST to be a main driver of LCC and T_{adv} a secondary contributor on inter-annual timescales. Additionally, they also suggest that SST and EIS are followers of LCC variation on such a short timescale. This implies that the SST has a potential to actively modulate the LCC variation on inter-annual timescales, rather than on intra-seasonal timescales. We conclude that, even in the summertime IJ2 region, S_{SSTF} variation related to the Oyashio Extension can actively control the monthly-mean anomalies of COT and SWCRE via, not the anomalous atmospheric circulation (i.e. T_{adv}), but rather via direct SST anomalies induced by a change in the western boundary currents. They indicate similar results to those obtained in Fig. 12, while the MLR model could not adequately capture the spatial characteristics of low-level cloud responses on a small spatial scale (i.e., a frontal scale at a Δ latitude of around 0°).

5 Summary and discussion

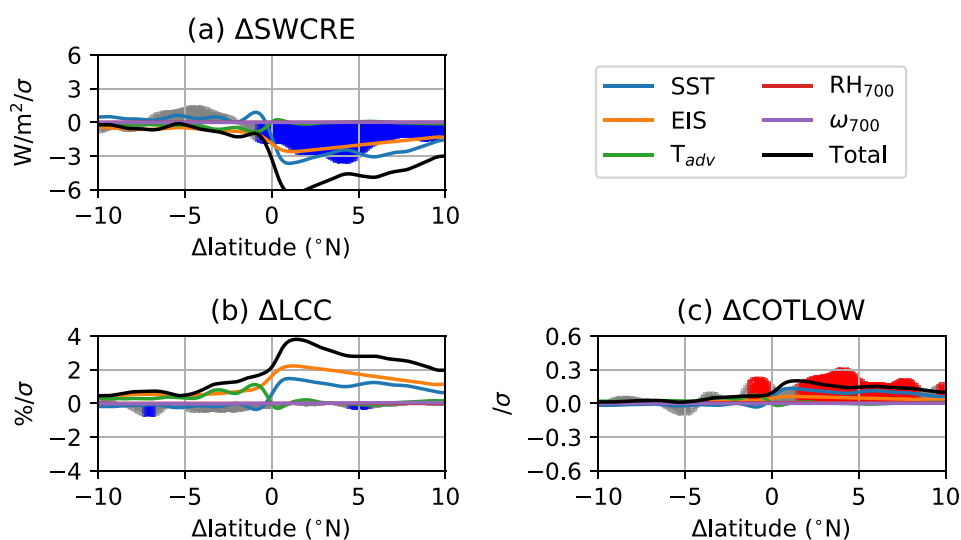
This study investigated the response of the properties of summertime low-level cloud to the properties of the SSTF (i.e., the strength of SST front; S_{SSTF}) associated with the Oyashio Extension in the WNP on inter-annual timescales, using satellite observational data, an atmospheric reanalysis dataset, and Argo float observations. The mechanisms responsible for the inter-annual variation of S_{SSTF} was investigated in detail before calculating the low-level cloud response to this variable. The results indicate that there is a strong contribution from the western boundary currents (i.e., the Kuroshio and Oyashio Extensions) to changes in the SSTF properties in the summertime WNP, while atmospheric forcing is the dominant contributing factor across a wide area of the CNP. The response of low-level cloud to the ocean-induced variation in the S_{SSTF} showed that negative SWCRE with more COT in the northern flank of the IJ2 SSTF can be induced by cold SST anomalies along with Oyashio Extension. Furthermore, the low-level cloud responses to the S_{SSTF} were examined using a multi-linear regression model to quantify the contributions from SST and other atmospheric factors (e.g., EIS and T_{adv}). The results of this model suggest that the local SST anomaly is a primary factor controlling the COT and SWCRE responses to the S_{SSTF} in summertime. However, other atmospheric controlling factors make only minor contributions.

Although the variation in the S_{SSTF} might be related to oceanic forcing, the SST anomaly also seems to be forced by the SWCRE of low-level cloud due to the positive feedback loop between the SST and low-level cloud properties (Norris and Leovy 1994). Using the HF term in the mixed-layer temperature budget equation (Moisan and Niiler 1998), we estimated how SST can be forced by ΔSWCRE ; the ratio of

the estimated ΔSST to the actual ΔSST shown in Fig. 13. As shown in Figs. 9a and 10a, positive (negative) ΔSWCRE appears in the southern (northern) flank of the SSTF, which induces warming (cooling) of the SST when the S_{SSTF} is high. Thermodynamically, the meridional distribution of ΔSWCRE induced by ΔSST can enhance S_{SSTF} within the positive feedback loop. However, we found no significant correlation between S_{SSTF} in the meridional direction and the meridional gradient of the SW directly over the SSTF (the IJ2 region in Fig. 8). This implies that there is no robust observational evidence for the feedback between S_{SSTF} and the SWCRE induced by low-level cloud just around the SSTF. However, far away from the SSTF in both flanks of the IJ2 SSTF (around 35°N or 45°N), ΔSWCRE -induced ΔSST can explain about half of the actual ΔSST . The area-mean ratios of the SST response in the northern and southern flanks of the IJ2 SSTF are 51% and 47%, respectively (Fig. 13b). In other words, the large-scale characteristics of the SST can be modulated by the radiative effect of low-level cloud, but the primary driver for frontal ΔSST might be oceanic forcing associated with the western boundary currents. It is also hard to assume that T_{sub} anomaly at deeper part was modulated by the radiative flux anomaly with changes in the low-level cloud properties. This represents further evidence of the active role of the SST anomaly in modulating low-level cloud.

On inter-annual timescales, several previous studies have found a significant linkage between the westerly jet and SSTF in the mid-latitude (e.g. Nakamura et al. 2004, 2008; Ogawa et al. 2012; Wang et al. 2019; Chen et al. 2019; Parfitt and Kwon 2020) via baroclinicity modulation processes. The dynamical state associated with a fluctuation of the jet position is one of the important drivers of the mid-latitude cloud variability. Low-level cloud responses to inter-annual variations of the positions of the jet and Hadley cell edge

Fig. 12 As in Fig. 9, but for the total response estimated using the multi-linear regression model (Total), and the contributions of each controlling factor of the local low-level cloud cover (sea surface temperature [SST], estimated inversion strength [EIS], horizontal air-temperature advection [T_{adv}], relative humidity at 700 hPa [RH_{700}], and vertical pressure velocity at 700 hPa [ω_{700}]) are also plotted



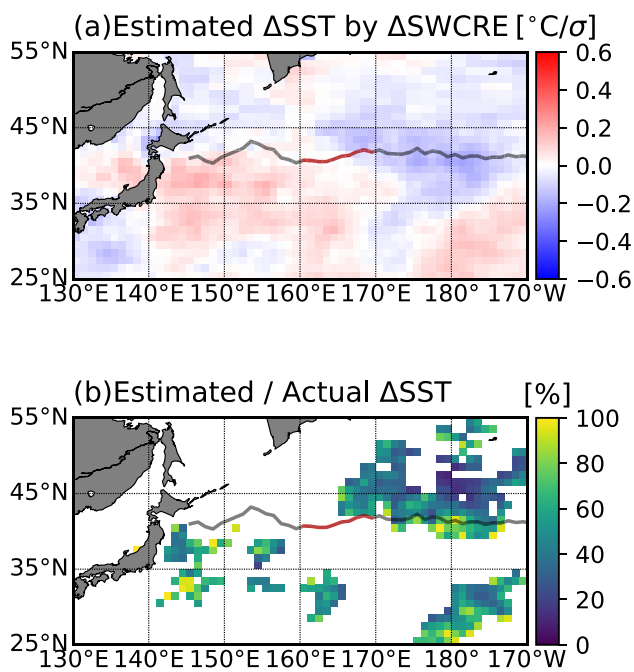


Fig. 13 Horizontal map of **a** estimated sea surface temperature (SST) response modulated by the shortwave cloud radiative effect (SWCRE) response shown in Fig. 4.10c, using the mixed-layer temperature equation for the increased strength of the sea surface temperature, **b** the ratio of the estimated SST response to the actual response (shown in Fig. 4.5) (unit: %). Only positive ratios are shown. The area-mean ratio of the SST response in the northern (southern) flank of the Isovich Jet 2 SST front (165–175° E) is 51% (47%)

have also been examined using the satellite observational records and CMIP experiments (Tselioudis et al. 2016; Grise and Medeiros 2016; Lipat et al. 2017; Zelinka et al. 2018). They showed that both dynamical and thermodynamical factors—i.e. anomalies of T_{adv} and EIS, respectively—can be the driver of low-level cloud responses to the jet fluctuations, although the primary factor is still under debate. While the present study focused on only the SSTF properties, we concluded that the local thermodynamical factors (i.e. SST and/or EIS) play key roles in modulating the low-level cloud variability around the Oyashio Extension in summertime. To fully understand the inter-annual variability of low-level cloud properties in the mid-latitude, we need to further investigate the relative contributions from the dynamical and thermodynamical components.

Finally, it is useful to comment on the spatial–temporal scales in the processes of the low-level cloud response to the SST front variations presented in this study. In terms of the spatial scales, our analysis was conducted using the cloud datasets with 1° horizontal resolution. This presents the difficulty in depicting the impact on low-level cloud properties on a SST frontal scale. Our recent work (Takahashi et al. 2020) investigated the sensitivity of low-level

cloud properties to the increased S_{SSTF} using Weather Research and Forecasting numerical simulations with different SST boundary conditions. The results suggested that the SSTF impact on low-level cloud can be explained by not only one-dimensional vertical process, but also two-dimensional horizontal processes with air-mass advection across the front (Schneider and Qiu 2015; Kilpatrick et al., 2014, 2016; Bai et al. 2019). However, its impact is limited within a hundred kilometer from the front position. In other words, the impacts of SST anomalies on larger spatial scale than the frontal scale can be mostly explained by the vertical process with local SST anomalies. Thus, our results in the present study are limited to depict the impacts of only local SST anomalies along the western boundary currents. In terms of time scales, the dominant timescale of the low-level cloud variability is shorter than inter-annual (e.g. de Szoeke et al. 2016). Atmospheric synoptic disturbances in the mid-latitude NP strongly affect the short-term variability of low-level clouds (Xu et al. 2005; Norris and Iacobellis 2005; Takahashi and Hayasaka 2020). In addition to the atmospheric variability, oceanic eddies can also affect cloud formation in atmospheric boundary layer via vertical mixing and pressure adjustment mechanisms, as shown in recent studies based on research cruise observations (Kawai et al. 2015, 2019; Jiang et al. 2019). Such synoptic timescale air-sea interactions are difficult to investigate using the coarse temporal observational datasets, and they are also not represented well in general circulation models. Future research is needed to examine the detailed spatial and temporal characteristics of the interaction among the synoptic disturbances, oceanic state, and cloud using a new generation of geostationary satellites with higher spatial–temporal resolutions.

Acknowledgements This work was supported by a Grant-in-Aid for the Japan Society for the Promotion of Science (JSPS) Research Fellow JP18J10606 and a Grant-in-Aid for Scientific Research (B) 16H04046 from the JSPS. The Aqua/MODIS Cloud Daily L3 Global 1 Deg. CMG dataset was acquired from the Level-1 and Atmosphere Archive Distribution System (LAADS) Distributed Active Archive Center (DAAC), located in the Goddard Space Flight Center in Greenbelt, Maryland (<https://ladsweb.nascom.nasa.gov/>). CERES data were obtained from the NASA Langley Research Center CERES ordering tool at <http://ceres.larc.nasa.gov/>. OISST data were provided by NOAA. The global ocean heat flux and evaporation data provided by the Woods Hole Oceanographic Institution OaFlux project (<http://oafux.whoi.edu>, last access: 06 November 2018) were funded by the NOAA Climate Observations and Monitoring (COM) program. ERA-Interim data were downloaded from the ECMWF data server at <http://apps.ecmwf.int/datasets/>. Roemmich-Gilson Argo Climatology dataset was provided by Scripps Institution of Oceanography (http://sio-argo.ucsd.edu/RG_Climatology.html). These data were collected and made freely available by the International Argo Program and the national programs that contribute to it. (<http://www.argo.ucsd.edu>, <http://argo.jcommops.org>). The Argo Program is part of the Global Ocean Observing System. The author thanks Kelvin Richards and Niklas Schneider from the University of Hawaii at Manoa for their helpful comments and discussion.

References

- Argo (2000) Argo float data and metadata from Global Data Assembly Centre (Argo GDAC). SEANOE. <https://doi.org/10.17882/42182>
- Bretherton CS, Blosser PN, Jones CR (2013) Mechanisms of marine low cloud sensitivity to idealized climate perturbations: A single-LES exploration extending the CGILS cases. *J Adv Model Earth Syst* 5:316–337. <https://doi.org/10.1002/jame.20019>
- Brient F, Schneider T (2016) Constraints on climate sensitivity from space-based measurements of low-cloud reflection. *J Clim* 29:5821–5835. <https://doi.org/10.1175/JCLI-D-15-0897.1>
- Chelton DB (2004) Satellite measurements reveal persistent small-scale features in ocean winds. *Science* (80-) 303:978–983. <https://doi.org/10.1126/science.1091901>
- Chen Q, Hu H, Ren X, Yang X (2019) Numerical simulation of midlatitude upper-level zonal wind response to the change of North Pacific subtropical front strength. *J Geophys Res Atmos* 124:4891–4912. <https://doi.org/10.1029/2018JD029589>
- Cronin MF, Bond NA, Thomas Farrar J et al (2013) Formation and erosion of the seasonal thermocline in the Kuroshio Extension Recirculation Gyre. *Deep Sea Res Part II Top Stud Oceanogr* 85:62–74. <https://doi.org/10.1016/j.dsr2.2012.07.018>
- de Szoeke SP, Verlinden KL, Yuter SE, Mechem DB (2016) The time scales of variability of marine low clouds. *J Clim* 29:6463–6481. <https://doi.org/10.1175/JCLI-D-15-0460.1>
- Dee DP, Uppala SM, Simmons AJ et al (2011) The ERA-Interim reanalysis: configuration and performance of the data assimilation system. *Q J R Meteorol Soc* 137:553–597. <https://doi.org/10.1002/qj.828>
- Frankignoul C, Sennéchal N, Kwon Y-O, Alexander MA (2011) Influence of the meridional shifts of the Kuroshio and the Oyashio extensions on the atmospheric circulation. *J Clim* 24:762–777. <https://doi.org/10.1175/2010JCLI3731.1>
- Grise KM, Medeiros B (2016) Understanding the varied influence of midlatitude jet position on clouds and cloud radiative effects in observations and global climate models. *J Clim* 29:9005–9025. <https://doi.org/10.1175/JCLI-D-16-0295.1>
- Hartmann DL, Short DA (1980) On the use of earth radiation budget statistics for studies of clouds and climate. *J Atmos Sci* 37:1233–1250. [https://doi.org/10.1175/1520-0469\(1980\)037%3c1233:OTUOER%3e2.0.CO;2](https://doi.org/10.1175/1520-0469(1980)037%3c1233:OTUOER%3e2.0.CO;2)
- Hayes SP, McPhaden MJ, Wallace JM (1989) The influence of sea-surface temperature on surface wind in the eastern equatorial Pacific: weekly to monthly variability. *J Clim* 2:1500–1506. [https://doi.org/10.1175/1520-0442\(1989\)002%3c1500:TIOSS%3e2.0.CO;2](https://doi.org/10.1175/1520-0442(1989)002%3c1500:TIOSS%3e2.0.CO;2)
- Hersbach H, Bell B, Berrisford P et al (2020) The ERA5 global reanalysis. *Q J R Meteorol Soc*. <https://doi.org/10.1002/qj.3803>
- Hosoda S, Nonaka M, Sasai Y, Sasaki H (2016) Early summertime interannual variability in surface and subsurface temperature in the North Pacific. In: “Hot Spots” in the climate system. Springer Japan, Tokyo, pp 91–107. https://doi.org/10.1007/978-4-431-56053-1_6
- Isoguchi O, Kawamura H, Oka E (2006) Quasi-stationary jets transporting surface warm waters across the transition zone between the subtropical and the subarctic gyres in the North Pacific. *J Geophys Res* 111:C10003. <https://doi.org/10.1029/2005JC003402>
- Jiang Y, Zhang S, Xie S et al (2019) Effects of a cold ocean eddy on local atmospheric boundary layer near the kuroshio extension. In situ observations and model experiments. *J Geophys Res Atmos* 124:5779–5790. <https://doi.org/10.1029/2018JD029382>
- Kato S, Rose FG, Rutan DA et al (2018) Surface irradiances of edition 4.0 clouds and the earth’s radiant energy system (CERES) energy balanced and filled (EBAF) data product. *J Clim* 31:4501–4527. <https://doi.org/10.1175/JCLI-D-17-0523.1>
- Kawai Y, Miyama T, Iizuka S et al (2015) Marine atmospheric boundary layer and low-level cloud responses to the Kuroshio Extension front in the early summer of 2012: three-vessel simultaneous observations and numerical simulations. *J Oceanogr* 71:511–526. <https://doi.org/10.1007/s10872-014-0266-0>
- Kawai H, Koshiro T, Webb MJ (2017) Interpretation of factors controlling low cloud cover and low cloud feedback using a unified predictive index. *J Clim* 30:9119–9131. <https://doi.org/10.1175/JCLI-D-16-0825.1>
- Kawai Y, Nishikawa H, Oka E (2019) In situ evidence of low-level atmospheric responses to the Oyashio front in early spring. *J Meteorol Soc Jpn Ser II* 97:423–438. <https://doi.org/10.2151/jmsj.2019-024>
- Kazmin AS (2016) The frontal system at the boundary of the East China Sea: its variability and response to large-scale atmospheric forcing. *Oceanology* 56:465–469. <https://doi.org/10.1134/S000143701604007X>
- Klein SA, Hartmann DL (1993) The seasonal cycle of low stratiform clouds. *J Clim* 6:1587–1606. [https://doi.org/10.1175/1520-0442\(1993\)006%3c1587:TSCOLS%3e2.0.CO;2](https://doi.org/10.1175/1520-0442(1993)006%3c1587:TSCOLS%3e2.0.CO;2)
- Klein SA, Hall A, Norris JR, Pincus R (2017) Low-cloud feedbacks from cloud-controlling factors: a review. *Surv Geophys* 38:1307–1329. <https://doi.org/10.1007/s10712-017-9433-3>
- Koshiro T, Yukimoto S, Shiotani M (2017) Interannual variability in low stratiform cloud amount over the summertime North Pacific in terms of cloud types. *J Clim* 30:6107–6121. <https://doi.org/10.1175/JCLI-D-16-0898.1>
- Kubar TL, Waliser DE, Li J-L, Jiang X (2012) On the annual cycle, variability, and correlations of oceanic low-topped clouds with large-scale circulation using aqua MODIS and ERA-interim. *J Clim* 25:6152–6174. <https://doi.org/10.1175/JCLI-D-11-00478.1>
- Kwon Y-O, Alexander MA, Bond NA et al (2010) Role of the gulf stream and Kuroshio-Oyashio systems in large-scale atmosphere-ocean interaction: a review. *J Clim* 23:3249–3281. <https://doi.org/10.1175/2010JCLI3343.1>
- Li J, Huang J, Stamnes K et al (2015) A global survey of cloud overlap based on CALIPSO and CloudSat measurements. *Atmos Chem Phys* 15:519–536. <https://doi.org/10.5194/acp-15-519-2015>
- Lindzen RS, Nigam S (1987) On the role of sea surface temperature gradients in forcing low-level winds and convergence in the tropics. *J Atmos Sci* 44:2418–2436. [https://doi.org/10.1175/1520-0469\(1987\)044%3c2418:OTROSS%3e2.0.CO;2](https://doi.org/10.1175/1520-0469(1987)044%3c2418:OTROSS%3e2.0.CO;2)
- Lipat B, Tselioudis G, Grise K, Polvani L (2017) CMIP5 models’ shortwave cloud radiative response and climate sensitivity linked to the climatological Hadley cell extent. *Geophys Res Lett* 44(11):5739–5748. <https://doi.org/10.1002/2017GL073151>
- Liu J-W, Xie S-P, Norris JR, Zhang S-P (2014) Low-level cloud response to the gulf stream front in winter using CALIPSO. *J Clim* 27:4421–4432. <https://doi.org/10.1175/JCLI-D-13-00469.1>
- Loeb NG, Doelling DR, Wang H et al (2018) Clouds and the earth’s radiant energy system (CERES) energy balanced and filled (EBAF) top-of-atmosphere (TOA) edition-4.0 DATA PRODUCT. *J Clim* 31:895–918. <https://doi.org/10.1175/JCLI-D-17-0208.1>
- Ma X, Chang P, Saravanan R et al (2017) Importance of resolving Kuroshio front and eddy influence in simulating the north pacific storm track. *J Clim* 30:1861–1880. <https://doi.org/10.1175/JCLI-D-16-0154.1>
- Masunaga R, Nakamura H, Miyasaka T et al (2015) Separation of climatological imprints of the Kuroshio extension and oyashio fronts on the wintertime atmospheric boundary layer: their sensitivity to SST resolution prescribed for atmospheric reanalysis. *J Clim* 28:1764–1787. <https://doi.org/10.1175/JCLI-D-14-00314.1>

- Masunaga R, Nakamura H, Miyasaka T et al (2016) Interannual modulations of oceanic imprints on the wintertime atmospheric boundary layer under the changing dynamical regimes of the kuroshio extension. *J Clim* 29:3273–3296. <https://doi.org/10.1175/JCLI-D-15-0545.1>
- Masunaga R, Nakamura H, Taguchi B, Miyasaka T (2020) Processes shaping the frontal-scale time-mean surface wind convergence patterns around the kuroshio extension in winter. *J Clim* 33:3–25. <https://doi.org/10.1175/JCLI-D-19-0097.1>
- McCoy DT, Eastman R, Hartmann DL, Wood R (2017) The change in low cloud cover in a warmed climate inferred from AIRS, MODIS, and ERA-interim. *J Clim* 30:3609–3620. <https://doi.org/10.1175/JCLI-D-15-0734.1>
- Minobe S, Takebayashi S (2015) Diurnal precipitation and high cloud frequency variability over the Gulf Stream and over the Kuroshio. *Clim Dyn* 44:2079–2095. <https://doi.org/10.1007/s00382-014-2245-y>
- Minobe S, Miyashita M, Kuwano-Yoshida A et al (2010) Atmospheric response to the gulf stream: seasonal variations. *J Clim* 23:3699–3719. <https://doi.org/10.1175/2010JCLI3359.1>
- Miyamoto A, Nakamura H, Miyasaka T (2018) Influence of the subtropical high and storm track on low-cloud fraction and its seasonality over the South Indian Ocean. *J Clim* 31:4017–4039. <https://doi.org/10.1175/JCLI-D-17-0229.1>
- Moisan JR, Niiler PP (1998) The seasonal heat budget of the North Pacific: net heat flux and heat storage rates (1950–1990). *J Phys Oceanogr* 28:401–421. [https://doi.org/10.1175/1520-0485\(1998\)028%3c0401:TSHBOT%3e2.0.CO;2](https://doi.org/10.1175/1520-0485(1998)028%3c0401:TSHBOT%3e2.0.CO;2)
- Myers TA, Norris JR (2013) Observational evidence that enhanced subsidence reduces subtropical marine boundary layer cloudiness. *J Clim* 26:7507–7524. <https://doi.org/10.1175/JCLI-D-12-00736.1>
- Myers TA, Norris JR (2015) On the relationships between subtropical clouds and meteorology in observations and CMIP3 and CMIP5 models. *J Clim* 28:2945–2967. <https://doi.org/10.1175/JCLI-D-14-00475.1>
- Myers TA, Norris JR (2016) Reducing the uncertainty in subtropical cloud feedback. *Geophys Res Lett* 43:2144–2148. <https://doi.org/10.1002/2015GL067416>
- Myers TA, Mechoso CR, DeFlorio MJ (2018) Coupling between marine boundary layer clouds and summer-to-summer sea surface temperature variability over the North Atlantic and Pacific. *Clim Dyn* 50:955–969. <https://doi.org/10.1007/s00382-017-3651-8>
- Nakamura H, Kazmin AS (2003) Decadal changes in the North Pacific oceanic frontal zones as revealed in ship and satellite observations. *J Geophys Res* 108:3078. <https://doi.org/10.1029/1999JC000085>
- Nakamura H, Yamagata T (1999) *Beyond El Niño*. Springer Berlin Heidelberg, Berlin
- Nakamura H, Sampe T, Tanimoto Y, Shimpo A (2004) Observed associations among storm tracks, jet streams, and midlatitude ocean fronts. In: *Geophysical Monograph Series*, vol. 147, pp 329–345. <https://doi.org/10.1029/147GM18>
- Nakamura H, Sampe T, Goto A et al (2008) On the importance of midlatitude oceanic frontal zones for the mean state and dominant variability in the tropospheric circulation. *Geophys Res Lett* 35:L15709. <https://doi.org/10.1029/2008GL034010>
- Nonaka M, Xie S-P (2003) Covariations of sea surface temperature and wind over the Kuroshio and its extension: evidence for ocean-to-atmosphere feedback. *J Clim* 16:1404–1413. [https://doi.org/10.1175/1520-0442\(2003\)16%3c1404:COSSTA%3e2.0.CO;2](https://doi.org/10.1175/1520-0442(2003)16%3c1404:COSSTA%3e2.0.CO;2)
- Norris JR, Iacobellis SF (2005) North Pacific cloud feedbacks inferred from synoptic-scale dynamic and thermodynamic relationships. *J Clim* 18:4862–4878. <https://doi.org/10.1175/JCLI3558.1>
- Norris JR, Leovy CB (1994) interannual variability in stratiform cloudiness and sea surface temperature. *J Clim* 7:1915–1925. [https://doi.org/10.1175/1520-0442\(1994\)007%3c1915:IVISCA%3e2.0.CO;2](https://doi.org/10.1175/1520-0442(1994)007%3c1915:IVISCA%3e2.0.CO;2)
- Norris JR, Zhang Y, Wallace JM (1998) Role of low clouds in summertime atmosphere-ocean interactions over the North Pacific. *J Clim* 11:2482–2490. [https://doi.org/10.1175/1520-0442\(1998\)011%3c2482:ROLICIS%3e2.0.CO;2](https://doi.org/10.1175/1520-0442(1998)011%3c2482:ROLICIS%3e2.0.CO;2)
- O'Reilly CH, Czaja A (2015) The response of the Pacific storm track and atmospheric circulation to Kuroshio Extension variability. *Q J R Meteorol Soc* 141:52–66. <https://doi.org/10.1002/qj.2334>
- Ogawa F, Spengler T (2019) Prevailing surface wind direction during air-sea heat exchange. *J Clim* 32:5601–5617. <https://doi.org/10.1175/JCLI-D-18-0752.1>
- Ogawa F, Nakamura H, Nishii K et al (2012) Dependence of the climatological axial latitudes of the tropospheric westerlies and storm tracks on the latitude of an extratropical oceanic front. *Geophys Res Lett* 39:1–5. <https://doi.org/10.1029/2011GL049922>
- Ogawa F, Nakamura H, Nishii K et al (2016) Importance of midlatitude oceanic frontal zones for the annular mode variability: interbasin differences in the southern annular mode signature. *J Clim* 29:6179–6199. <https://doi.org/10.1175/JCLI-D-15-0885.1>
- Ohishi S, Tozuka T, Cronin MF (2017) Frontogenesis in the agulhas return current region simulated by a high-resolution CGCM. *J Phys Oceanogr* 47:2691–2710. <https://doi.org/10.1175/JPO-D-17-0038.1>
- Okajima S, Nakamura H, Nishii K et al (2014) Assessing the importance of prominent warm SST anomalies over the midlatitude North Pacific in forcing large-scale atmospheric anomalies during 2011 summer and autumn. *J Clim* 27:3889–3903. <https://doi.org/10.1175/JCLI-D-13-00140.1>
- Parfitt R, Kwon Y-O (2020) The modulation of gulf stream influence on the troposphere by the eddy-driven jet. *J Clim* 33:4109–4120. <https://doi.org/10.1175/JCLI-D-19-0294.1>
- Parfitt R, Seo H (2018) A new framework for near-surface wind convergence over the kuroshio extension and Gulf Stream in wintertime: the role of atmospheric fronts. *Geophys Res Lett* 45:9909–9918. <https://doi.org/10.1029/2018GL080135>
- Platnick S (2015) MYD08 _ D3 - MODIS / Aqua Aerosol Cloud Water Vapor Ozone Daily L3 Global 1Deg CMG. https://doi.org/10.5067/MODIS/MYD08_D3.061
- Qiu B (2001) Kuroshio and Oyashio currents. In: *Encyclopedia of ocean sciences*. Elsevier, pp 358–369. <https://doi.org/10.1016/B978-0-12-409548-9.11295-3>
- Qiu B, Chen S, Schneider N (2017) Dynamical links between the decadal variability of the oyashio and kuroshio extensions. *J Clim* 30:9591–9605. <https://doi.org/10.1175/JCLI-D-17-0397.1>
- Qu X, Hall A, Klein SA, DeAngelis AM (2015) Positive tropical marine low-cloud cover feedback inferred from cloud-controlling factors. *Geophys Res Lett* 42:7767–7775. <https://doi.org/10.1002/2015GL065627>
- Reynolds RW, Rayner NA, Smith TM et al (2002) An improved in situ and satellite SST analysis for climate. *J Clim* 15:1609–1625. [https://doi.org/10.1175/1520-0442\(2002\)015%3c1609:AIHSA%3e2.0.CO;2](https://doi.org/10.1175/1520-0442(2002)015%3c1609:AIHSA%3e2.0.CO;2)
- Roemmich D, Gilson J (2009) The 2004–2008 mean and annual cycle of temperature, salinity, and steric height in the global ocean from the Argo Program. *Prog Oceanogr* 82:81–100. <https://doi.org/10.1016/j.pocean.2009.03.004>
- Sasaki YN, Yamada Y (2018) Atmospheric response to interannual variability of sea surface temperature front in the East China Sea in early summer. *Clim Dyn* 51:2509–2522. <https://doi.org/10.1007/s00382-017-4025-y>
- Schmidtko S, Johnson GC, Lyman JM (2013) MIMOC: A global monthly isopycnal upper-ocean climatology with mixed layers. *J Geophys Res Ocean* 118:1658–1672. <https://doi.org/10.1002/jgrc.20122>

- Seethala C, Norris JR, Myers TA (2015) How has subtropical stratocumulus and associated meteorology changed since the 1980s? *J Clim* 28:8396–8410. <https://doi.org/10.1175/JCLI-D-15-0120.1>
- Shimada T, Minobe S (2011) Global analysis of the pressure adjustment mechanism over sea surface temperature fronts using AIRS/Aqua data. *Geophys Res Lett*. <https://doi.org/10.1029/2010GL046625>
- Smirnov D, Newman M, Alexander MA et al (2015) Investigating the local atmospheric response to a realistic shift in the oyashio sea surface temperature front. *J Clim* 28:1126–1147. <https://doi.org/10.1175/JCLI-D-14-00285.1>
- Sugimoto S, Kobayashi N, Hanawa K (2014) Quasi-decadal variation in intensity of the western part of the winter subarctic SST front in the Western North Pacific: the influence of Kuroshio Extension Path State. *J Phys Oceanogr* 44:2753–2762. <https://doi.org/10.1175/JPO-D-13-0265.1>
- Takahashi N, Hayasaka T (2020) Air-sea interactions among oceanic low-level cloud, sea surface temperature, and atmospheric circulation on an intraseasonal time scale in the summertime North Pacific based on satellite data analysis. *J Clim* 33:9195–9212. <https://doi.org/10.1175/JCLI-D-19-0670.1>
- Takahashi N, Hayasaka T, Manda A, Schneider N (2020) Impact of the oyashio extension sst front on synoptic variability of oceanic low-level cloud in summertime based on WRF numerical simulation. *J Geophys Res Atmos*. <https://doi.org/10.1029/2020JD032518>
- Tanimoto Y, Nakamura H, Kagimoto T, Yamane S (2003) An active role of extratropical sea surface temperature anomalies in determining anomalous turbulent heat flux. *J Geophys Res* 108:3304. <https://doi.org/10.1029/2002JC001750>
- Tanimoto Y, Xie SP, Kai K et al (2009) Observations of marine atmospheric boundary layer transitions across the summer Kuroshio extension. *J Clim* 22:1360–1374. <https://doi.org/10.1175/2008JCLI2420.1>
- Terai CR, Klein SA, Zelinka MD (2016) Constraining the low-cloud optical depth feedback at middle and high latitudes using satellite observations. *J Geophys Res Atmos* 121:9696–9716. <https://doi.org/10.1002/2016JD025233>
- Terai CR, Zhang Y, Klein SA et al (2019) Mechanisms behind the extratropical stratiform low-cloud optical depth response to temperature in ARM site observations. *J Geophys Res Atmos* 124:2127–2147. <https://doi.org/10.1029/2018JD029359>
- Tokinaga H, Tanimoto Y, Xie S-P et al (2009) Ocean frontal effects on the vertical development of clouds over the Western North Pacific. In situ and satellite observations. *J Clim* 22:4241–4260. <https://doi.org/10.1175/2009JCLI2763.1>
- Tomita H, Kouketsu S, Oka E, Kubota M (2011) Locally enhanced wintertime air-sea interaction and deep oceanic mixed layer formation associated with the subarctic front in the North Pacific. *Geophys Res Lett*. <https://doi.org/10.1029/2011GL049902>
- Tozuka T, Cronin MF (2014) Role of mixed layer depth in surface frontogenesis: the Agulhas Return Current front. *Geophys Res Lett* 41:2447–2453. <https://doi.org/10.1002/2014GL059624>
- Tozuka T, Cronin MF, Tomita H (2017) Surface frontogenesis by surface heat fluxes in the upstream Kuroshio Extension region. *Sci Rep* 7:10258. <https://doi.org/10.1038/s41598-017-10268-3>
- Tozuka T, Ohishi S, Cronin MF (2018) A metric for surface heat flux effect on horizontal sea surface temperature gradients. *Clim Dyn* 51:547–561. <https://doi.org/10.1007/s00382-017-3940-2>
- Tselioudis G, Lipat BR, Konsta D et al (2016) Midlatitude cloud shifts, their primary link to the Hadley cell, and their diverse radiative effects. *Geophys Res Lett* 43:4594–4601. <https://doi.org/10.1002/2016GL068242>
- Wallace JM, Mitchell TP, Deser C (1989) The influence of sea-surface temperature on surface wind in the Eastern Equatorial Pacific: seasonal and interannual variability. *J Clim* 2:1492–1499. [https://doi.org/10.1175/1520-0442\(1989\)002%3c1492:TIOSST%3e2.0.CO;2](https://doi.org/10.1175/1520-0442(1989)002%3c1492:TIOSST%3e2.0.CO;2)
- Wang L, Hu H, Yang X (2019) The atmospheric responses to the intensity variability of subtropical front in the wintertime North Pacific. *Clim Dyn* 52:5623–5639. <https://doi.org/10.1007/s00382-018-4468-9>
- Wood R (2012) Stratocumulus clouds. *Mon Weather Rev* 140:2373–2423. <https://doi.org/10.1175/MWR-D-11-00121.1>
- Wood R, Bretherton CS (2006) On the relationship between stratiform low cloud cover and lower-tropospheric stability. *J Clim* 19:6425–6432. <https://doi.org/10.1175/JCLI3988.1>
- Wu R, Kinter JL (2010) Atmosphere-ocean relationship in the midlatitude North Pacific: seasonal dependence and east-west contrast. *J Geophys Res* 115:D06101. <https://doi.org/10.1029/2009JD012579>
- Xie S-P (2004) Satellite observations of cool ocean-atmosphere interaction. *Bull Am Meteorol Soc* 85:195–208. <https://doi.org/10.1175/BAMS-85-2-195>
- Xu H, Xie S, Wang Y (2005) Subseasonal variability of the southeast pacific stratus cloud deck. *J Clim* 18:131–142. <https://doi.org/10.1175/JCLI3250.1>
- Yao Y, Zhong Z, Yang X-Q, Lu W (2017) An observational study of the North Pacific storm-track impact on the midlatitude oceanic front. *J Geophys Res Atmos* 122:6962–6975. <https://doi.org/10.1002/2016JD026192>
- Yu L, Jin X, Weller AR (2008) Multidecade Global Flux Datasets from the objectively analyzed air-sea fluxes (OAFlux) project: latent and sensible heat fluxes, ocean evaporation, and related surface meteorological variables
- Zelinka MD, Grise KM, Klein SA et al (2018) Drivers of the low-cloud response to poleward jet shifts in the north pacific in observations and models. *J Clim* 31:7925–7947. <https://doi.org/10.1175/JCLI-D-18-0114.1>
- Zhai C, Jiang JH, Su H (2015) Long-term cloud change imprinted in seasonal cloud variation: More evidence of high climate sensitivity. *Geophys Res Lett* 42:8729–8737. <https://doi.org/10.1002/2015GL065911>

Publisher's Note Springer Nature remains neutral with regard to jurisdictional claims in published maps and institutional affiliations.